applied sciences

MDPI

Article

Analysis of the Thermomechanical Fatigue Behavior of Fully Ferritic High Chromium Steel Crofer®22 H with Cyclic Indentation Testing

Bastian Blinn [1,*], David Görzen [1], Torsten Fischer [2], Bernd Kuhn [2] and Tilmann Beck [1]

[1] Institute of Materials Science and Engineering, TU Kaiserslautern, 67663 Kaiserslautern, Germany; goerzen@mv.uni-kl.de (D.G.); beck@mv.uni-kl.de (T.B.)

[2] Forschungszentrum Juelich GmbH, Institute of Energy and Climate Research (IEK), Microstructure and Properties of Materials (IEK-2), 52428 Juelich, Germany; t.fischer@fz-juelich.de (T.F.); b.kuhn@fz-juelich.de (B.K.)

* Correspondence: blinn@mv.uni-kl.de; Tel.: +49-631-205-5288

Received: 28 August 2020; Accepted: 11 September 2020; Published: 16 September 2020

Abstract: The 22 wt.% Cr, fully ferritic stainless steel Crofer®22 H has higher thermomechanical fatigue (TMF)- lifetime compared to advanced ferritic-martensitic P91, which is assumed to be caused by different damage tolerance, leading to differences in crack propagation and failure mechanisms. To analyze this, instrumented cyclic indentation tests (CITs) were used because the material's cyclic hardening potential—which strongly correlates with damage tolerance, can be determined by analyzing the deformation behavior in CITs. In the presented work, CITs were performed for both materials at specimens loaded for different numbers of TMF-cycles. These investigations show higher damage tolerance for Crofer®22 H and demonstrate changes in damage tolerance during TMF-loading for both materials, which correlates with the cyclic deformation behavior observed in TMF-tests. Furthermore, the results obtained at Crofer®22 H indicate an increase of damage tolerance in the second half of TMF-lifetime, which cannot be observed for P91. Moreover, CITs were performed at Crofer®22 H in the vicinity of a fatigue crack, enabling to locally analyze the damage tolerance. These CITs show differences between crack edges and the crack tip. Conclusively, the presented results demonstrate that CITs can be utilized to analyze TMF-induced changes in damage tolerance.

Keywords: cyclic hardening potential; damage tolerance; microstructural evolution; cyclic indentation test; thermomechanical fatigue; PhyBaL$_{CHT}$

1. Introduction

Because of the current dramatic changes in electricity generation and supply, conventional thermal power plants are operated in a more fluctuating way, resulting in a combination of creep and cyclic loading of the hot section components. As shown by Holdsworth et al. [1], this leads to accelerated crack propagation, and hence, reduces lifetime compared to pure creep loadings. For combined loading conditions, preliminary work at materials for thermal power plant applications [2] has shown, that 22 wt.% Cr, fully ferritic stainless steel Crofer®22 H exhibits a higher lifetime compared to advanced ferritic-martensitic (AFM) steel P91.

While strengthening of P91 is mainly achieved by $M_{23}C_6$ (M: Mo, Cr)- and MX (M: V, Nb; X: N)-particles, as well as solid solution and sub-grain hardening [3], the fully ferritic Crofer®22 H, can be strengthened by a combination of solid solution hardening and intermetallic Laves phase $(Fe,Cr,Si)_2(Nb,W)$ precipitates [4], whereby Crofer®22 H has a limited solubility of C and N in the ferritic matrix. For Crofer®22 H, the decisive factor for hardening in (thermomechanical) fatigue

loading is the thermomechanically induced precipitation of the Laves phase, which takes place during application in the temperature range from 600 to 700 °C [5].

Moreover, Crofer®22 H exhibits a stable grain structure under thermomechanical fatigue (TMF)-loading, which is in contrast to the AFM steels, showing unstable martensite lath structure and "polygonization" at TMF-loading conditions [5]. Additionally, in Reference [5], a higher damage tolerance of Crofer®22 H compared to P91 is indicated, leading to a higher TMF-lifetime for Crofer®22 H. Investigations at another fully ferritic, Laves phase strengthened steel [6] show a higher amount of hardening and additionally a sub-grain formation in front of the crack tip, resulting in crack branching or deflection at sub-grain boundaries and crack deflection at Laves phase particles [6]. Furthermore, it is assumed, that plastic deformation or high dislocation densities in the vicinity of a crack tip, as well as sub-grain boundaries, can boost the Laves phase precipitation, because both can act as nucleation sites [6].

As shown in Reference [5], the differences in fatigue behavior of both steel types are caused by different microstructural evolution. To quantify the microstructural evolution caused by cyclic loading, several experimental methods can be applied. Besides common microstructural characterization methods, e.g., scanning electron microscopy or transmission electron microscopy [7,8], further techniques, such as measuring the development of hardness or electrical resistivity at different fatigue states [8,9], can be used. In this context, Miroslav et al. [10] showed for the bainitic steel 24CrMoV55, as well as for the ferritic-pearlitic steel S355J0, that measuring hardness during fatigue tests serves as a suitable indicator to detect fatigue-induced microstructural changes.

In general, indentation tests constitute an efficient method to determine various mechanical properties, such as hardness or elastic modulus [11,12]. Furthermore, a material's cyclic properties can be characterized using cyclic indentation tests (CITs) [13–15]. As shown by Reference [15] for 100Cr6 and [13] for two copper alloyed steels with carbon contents of 0.005 and 0.21 wt-%, respectively, using CITs enables the determination of the material's cyclic hardening potential, which correlates with the amount of cyclic hardening detected in uniaxial fatigue tests. Additionally, preliminary work [16] demonstrates at differently heat-treated 42CrMo4, that the deformation behavior measured in CITs is in good accordance with the cyclic deformation behavior in uniaxial fatigue tests with compressive stresses ($R = -\infty$). Moreover, a strong correlation of cyclic hardening potential determined in CITs with the materials damage tolerance was found in References [17,18].

By reducing the indentation force, the indent diagonal (which has been shown to correlate with the plastically deformed volume under the indenter [19,20]) and indentation tests enable the analysis of locally restricted areas. As reported in Reference [16] for differently heat-treated 42CrMo4, as well as copper alloyed 18CrNiMo7-6, CITs with reduced indentation force can be used to detect local material properties with high spatial resolution. Moreover, Klein et al. [21] showed that for high-Mn TWIP steel, CITs are able to characterize hardness and cyclic hardening potential of different surface morphologies, which can be associated with the resulting fatigue behavior. Note that the indentation size effect (ISE) has to be considered when reducing the indentation force, and therefore, indentation depth [16]. The ISE means an increase of hardness with decreasing indentation depth and can be explained by the model of Nix and Gao [22].

As the TMF-tests performed in Reference [5] indicate a higher damage tolerance for Crofer®22 H in relation to P91, CITs were performed at various states of TMF-loading to elaborate the difference in damage tolerance, as well as its TMF-induced evolution. Additionally, local investigations of the damage tolerance in the vicinity of a fatigue crack were performed using CITs with reduced indentation force, thereby quantifying local differences in mechanical properties. Moreover, the underlying microstructural changes reported in Reference [5] are compared to the results obtained in CITs. Consequently, the results presented here are an extension of the investigations from Reference [5]. Whereas in Reference [5], the TMF-behavior of P91 and Crofer®22 H, as well as microstructural evolution, are analyzed, the presented work focuses the investigation of TMF-induced changes in cyclic hardening potential using a novel testing approach.

2. Materials

The advanced ferritic-martensitic (AFM) steel P91, belonging to the 9Cr-1Mo family of steels, is widely applied in current thermal power plants [23,24]. P91 has a tempered martensite structure after austenitization, air cooling, and tempering. As shown in Figure 1, the tempered martensite is characterized by prior austenite grain boundaries (PAGBs), as well as packet and lath boundaries [3]. The stability is achieved by precipitation (predominantly Cr and Mo-rich $M_{23}C_6$, M_7C_3, M_3C, M_2X, Cr_2N), solid solution, and sub-grain hardening [3]. $M_{23}C_6$ and MX precipitate along PAGBs lath boundaries, packet boundaries (see Figure 1), as well as inside intra-lath regions [3]. However, long-term stability during creep stress is deteriorated by the formation of the intermetallic Laves phase and Z-phase [3].

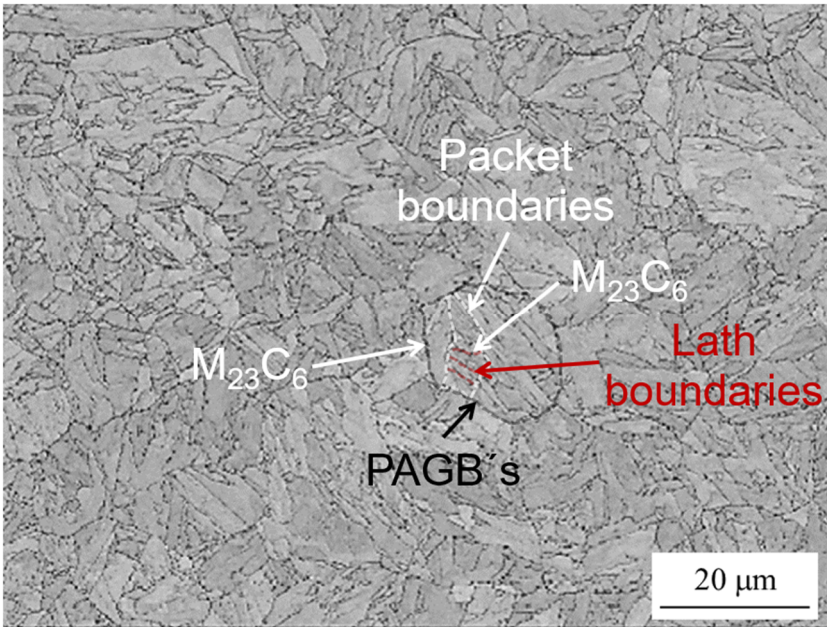

Figure 1. The characteristic microstructure of tempered ferritic-martensitic steel P91 [5]. PAGB, prior austenite grain boundaries.

The P91 investigated in the present study was extracted from a pipe section with an outer diameter of 160 mm and a wall thickness of 20 mm. Austenitization was carried out at 1050 °C for 0.5 h, followed by air cooling. Afterwards, tempering at 750 °C for 1 h and subsequent air cooling were performed.

The additionally investigated Crofer®22 H is a 22 wt.% Cr, fully ferritic stainless steel and was developed by a collaboration between Forschungszentrum Juelich GmbH, Germany, and VDM Metals GmbH, Germany [25]. It serves as a low-cost, metallic interconnector material for the light-weight design of solid oxide fuel cell stacks [26]. Figure 2 depicts a typical microstructure of recrystallized (1075 °C/22 min/air cooling), and subsequently, precipitation annealed (650 °C/2 h/water quenching) Crofer®22 H. Fine Laves phase particles are uniformly dispersed [27,28] in the matrix and additionally, the high angle grain boundaries (HAGBs) are covered by Laves phase. Furthermore, particle-free zones (PFZs) are formed along the HAGBs. The strength of the material is based on a combination of solid solution hardening and intermetallic $(Fe,Cr,Si)_2(Nb,W)$ Laves phase particle precipitation [4]. Moreover, thermomechanically triggered precipitation of the Laves phase particles [29,30] has a significant impact on TMF-behavior [5], and fatigue performance [6] of such Laves phase strengthened, ferritic steels. In addition to that, an excellent creep behavior in the temperature range of 600–650 °C has been demonstrated by Reference [4] for this type of steels.

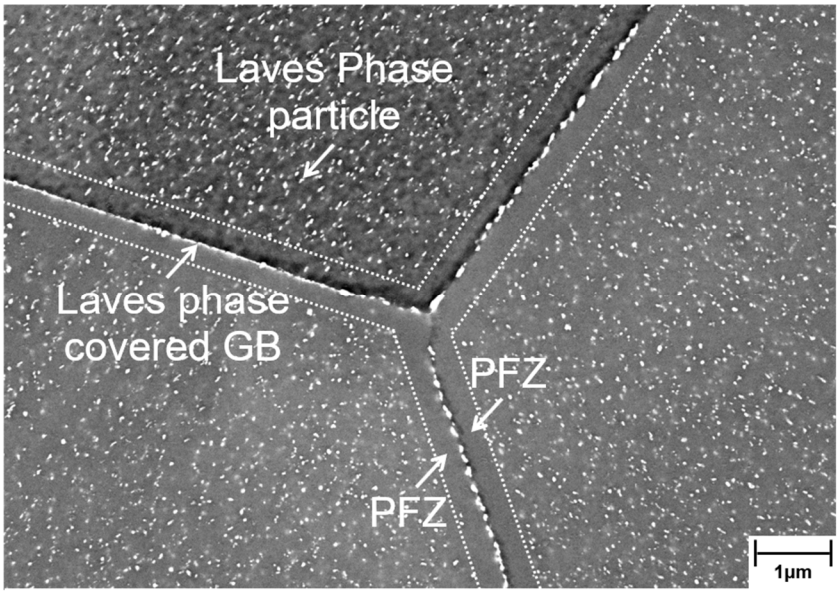

Figure 2. The microstructure of the fully ferritic Crofer®22 H steel in the precipitated state. PFZ, particle-free zones; GB, grain boundaries.

In the presented work, recrystallized (1050 °C/5+ minutes, depending on section thickness/rapid air-cooling) Crofer®22 H from VDM Metals, Germany was investigated.

The chemical compositions of Crofer®22 H were determined with inductively coupled plasma optical emission spectrometry and are given in Table 1, which also contains the chemical composition from the manufacturer's datasheet of P91. In Table 2, the typical mechanical properties at an ambient temperature of the as-delivered state are shown, respectively.

Table 1. Chemical compositions in wt.% of P91 and Crofer®22 H.

Material	C	N	Cr	Mn	Si	Nb	W	V	Al	Ni	Mo	La	Ti
P91	0.1	0.051	8.1	0.46	–	0.07	–	0.18	0.34	0.33	0.92	–	–
Crofer®22 H	<0.01	<0.01	22.93	0.43	0.21	0.51	1.94	–	–	–	–	0.08	0.07

Table 2. Typical mechanical properties of P91 and Crofer®22 H at ambient temperature in the as-delivered state.

Material	Yield Strength (MPa)	Tensile Strength (Mpa)	Hardness (HV_{10})
P91 (tubes [31])	≥415	620–850	≥190
Crofer®22 H (Sheet and plate ≤ 16 mm [32])	390	520	160–200

3. Methods

Total strain-controlled out-of-phase (oop) thermomechanical fatigue (TMF-) tests were performed in accordance with the European Code-of-Practice [33]. Therefore, cylindrical specimens with a gauge length of 15 mm and a diameter of 7 mm, as well as servo-hydraulic fatigue testing systems, equipped with inductive specimen heating systems, were used. For temperature control, a type R ribbon thermocouple was applied in the center of the gauge length. The strain was directly measured using high-temperature extensometers. All experiments were conducted in a temperature range from 250 to 650 °C with heating, as well as the cooling rate of dT/dt = 10 Ks^{-1}. To reduce creep deformation

to a minimum, no holding time was applied. To achieve the specified cooling rate, the specimens were directly cooled with compressed air after reaching the maximum temperature. Moreover, the resulting thermal strain ε_{th} was suppressed by applying a mechanical strain of $\varepsilon_{mech} = -\varepsilon_{th}$ in oop TMF cycles. Since the TMF cycle started at a minimum temperature of 250 °C, the strain ratio of mechanical strain was $R_{\varepsilon,\,mech} = -\infty$. The differently pronounced thermal expansion of P91 and Crofer®22 H, which is mainly caused by substantially different Cr content, leads to deviations in ε_{th}, and thus, in ε_{mech}. While P91 was loaded with $\varepsilon_{mech} = 0.54\%$, Crofer®22 H was charged with $\varepsilon_{mech} = 0.509\%$. Consequently, one may expect a higher stress range for P91, but in TMF tests, a higher stress level was observed for Crofer®22 H (see Figure 3), caused by pronounced Laves phase strengthening of Crofer®22 H (see Reference [5]). Moreover, both materials show a decrease in stress range during TMF-loading, which is more pronounced for Crofer22 H. The results of TMF-experiments are discussed in detail in Reference [5].

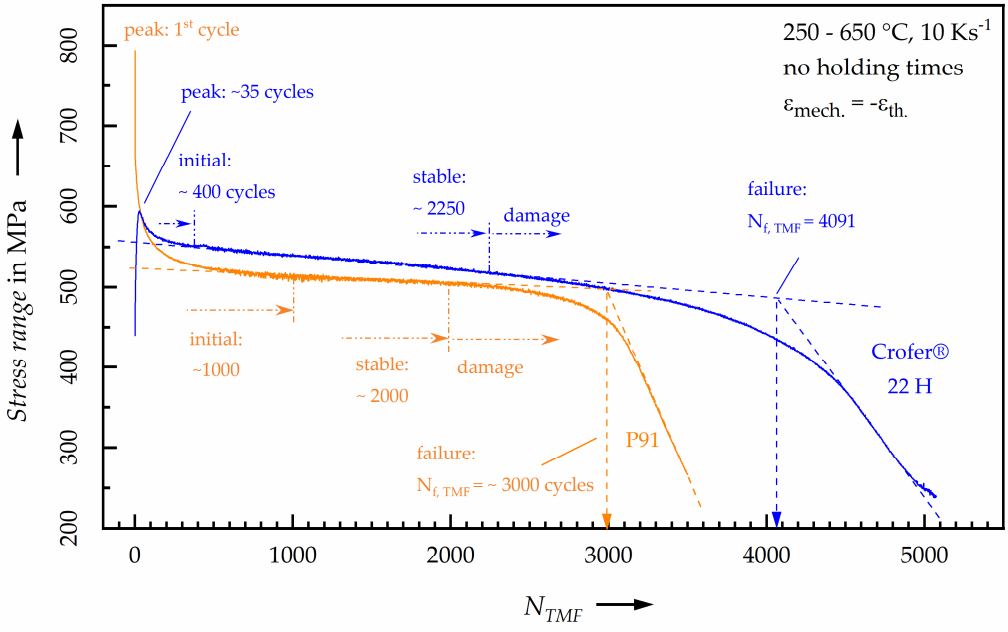

Figure 3. Evolution of stress range during oop-TMF loading of P91 and Crofer®22 H [5].

Despite slightly higher maximum stress, Crofer®22 H exhibits in Reference [5] higher TMF-lifetime in relation to P91 (see Figure 3), which might be explained by differently pronounced damage tolerance. To analyze the changes in cyclic hardening potential, which correlates with damage tolerance [17,18], during TMF-loading, instrumented cyclic indentation tests (CITs) were conducted at the initial state (IS), as well as after defined numbers of TMF-cycles N_{TMF}. Therefore, the CITs were performed in the volume of the gauge length of the respective specimen with a maximum indentation force of $F_{max} = 1000$ mN and in total ten indentation cycles with a frequency of $f = 1/12$ Hz. Because this requires a destructive preparation of the specimens' gauge length, different specimens were loaded for various N_{TMF}. For CITs, a Fischerscope H100C (Helmut Fischer GmbH, Germany), which enables continuous detection of the indentation depth h and indentation force F, was used.

Additionally, CITs were performed at the crack edges, as well as in front of the crack tip, and thus, in the plastic zone, which can be estimated according to Reference [34]. These measurements were conducted at a fatigue crack, observed at a specimen of Crofer®22 H loaded for 4342 TMF-cycles (see Figure 4a). In addition to $F_{max} = 1000$ mN, a maximum indentation force of 100 mN was used to get a higher resolution of the material volume around the fatigue crack (see Reference [16]).

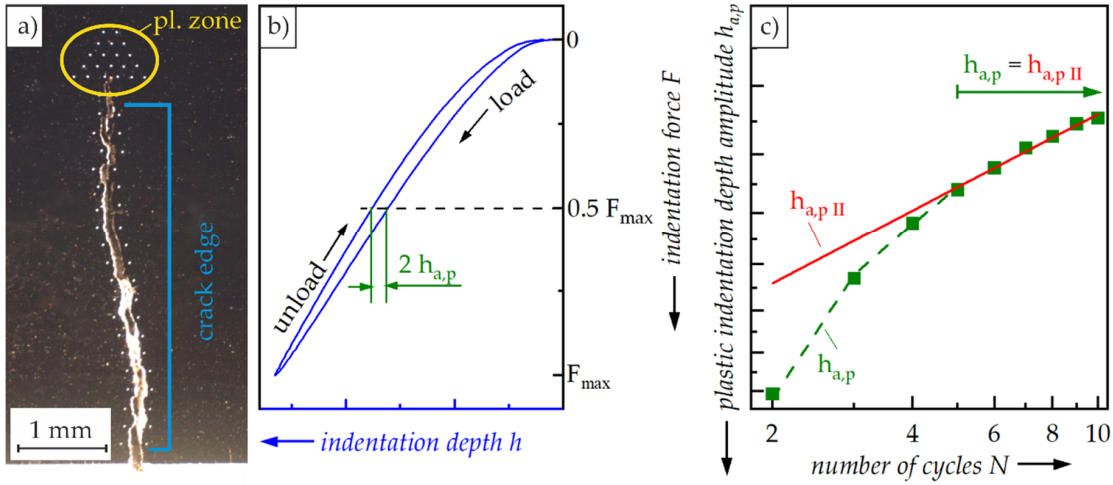

Figure 4. (**a**) Stereoscopic micrograph with indentation points at crack edges and crack tip; schematic description of (**b**) indentation force *F*-indentation depth *h* hysteresis, as well as plastic indentation depth amplitude $h_{a,p}$ and (**c**) $h_{a,p}$-N curves with $h_{a,p\ II}$ [13].

The CITs were evaluated using the PhyBaL$_{CHT}$ procedure presented in detail in References [13,15,16]. During indentation, the indentation force *F* and indentation depth *h* are measured continuously, revealing an *F*-*h* hysteresis from the 2nd cycle on (see Figure 4b). The half-width of the *F*-*h* hysteresis at mean loading is considered as a characteristic parameter to describe the deformation behavior and is called plastic indentation depth amplitude $h_{a,p}$. The $h_{a,p}$-N relation plotted schematically in Figure 4c, shows a slope change from the 5th cycle, which indicates saturation of macroplastic deformation, and hence, the deformation behavior in CITs is dominated by microplasticity in this regime. Consequently, the regime after the 5th cycle, which can further be described by the power-law function $h_{a,p\ II}$ (see Equation (1)), is analyzed to characterize the material's cyclic properties [15].

$$h_{a,p\ II} = a_{II} \cdot N^{e_{II}} \quad (1)$$

The slope of $h_{a,p\ II}$ indicates the amount of cyclic hardening during CIT and is described by the exponent e_{II}, called cyclic hardening exponent$_{CHT}$ [15]. A steeper slope results in a higher $|e_{II}|$, which implies a larger amount of cyclic hardening during indentation testing. In addition to that and in correspondence to conventional microhardness measurement, the Martens hardness (*HM*) can be determined from the *F*-*h* relation of the 1st cycle.

To obtain statistically reliable values of $h_{a,p}$-N curves, and *HM*, for each condition, mean values were determined using 40 indentation points, respectively. Note that for the measurements in the relatively small plastic zone in front of the crack tip, only 20 indentation points could be realized. For investigating the mechanical properties at the crack edges, 40 indentation points were utilized with F_{max} = 1000 mN, whereas a F_{max} = 100 mN enabled the possibility to perform 60 CITs along the crack edge. For analysis in the fatigue crack vicinity, CITs were performed along the fatigue crack (comp. Figure 4a) and on different planes prepared by grinding and polishing the sample. In Section 4, for each condition, the mean values and 90% confidence intervals, based on the overall number of indentation points, are shown.

4. Results and Discussion

4.1. Evolution of Cyclic Hardening Potential and Hardness During TMF Loading

The TMF-tests demonstrate, in spite of slightly larger stress range and mean stresses (91 MPa for CroFer®22 H and 75 MPa for P91), a higher lifetime for CroFer®22 H compared to P91 (see Figure 3). While P91 exhibits a strong degradation of its initial martensitic lath structure, called "polygonization",

the ferritic CroFer®22 H shows an increase of the Laves phase particle fraction, caused by TMF-loading and leading to a higher stress range and maximum stress in relation to P91 (see Figure 3 and [5]). These microstructural phenomena described in Reference [5] are dependent on the number of TMF-cycles N_{TMF} and influence the material's damage tolerance. To determine the evolution of damage tolerance during TMF-loading, CITs were performed at different N_{TMF}.

Although the TMF-tests were performed at variable, elevated temperatures, and thus, at different conditions compared to the CITs performed at ambient temperature, the CITs enable the determination of the evolution of the material's mechanical properties, i.e., hardness and cyclic hardening potential, resulting from TMF-loading. Note that cyclic hardening potential, represented by e_{II}, strongly correlates with the material's damage tolerance [17,18].

Comparing the materials in their initial states (IS), Crofer®22 H has lower hardness, but significantly higher cyclic hardening potential, compared to P91 (see Figure 5)—which correlates to stronger damage tolerance indicated in Reference [5]. Moreover, Crofer®22 H shows lower $h_{a,p}$ values in relation to P91, due to extensively more pronounced cyclic hardening during cyclic indentation (see Figure 6).

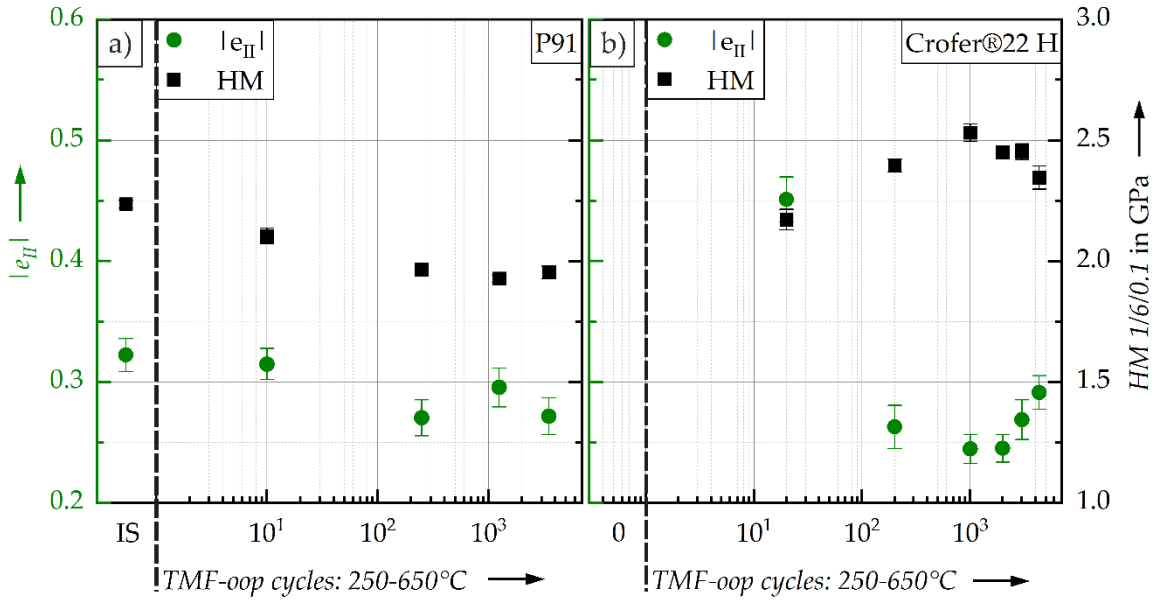

Figure 5. Cyclic hardening exponent$_{CHT}$ $|e_{II}|$ and martens hardness *HM* of the initial state (IS) and subject to TMF-cycles for (**a**) P91 and (**b**) Crofer®22 H.

For P91 a pronounced decrease of $|e_{II}|$ can be observed during the first 250 TMF-cycles, which is accompanied by a hardness decrease, correlating with the cyclic softening observed in TMF-experiments (comp. Figure 4, Figure 5 and [5]). However, from the 250th TMF-cycle on, P91 exhibits a stabilization of both hardness and $|e_{II}|$, which also correlates to the cyclic deformation curves shown in Figure 3, as well as the $h_{a,p}$-N curves in Figure 6. The degradation of martensite laths discussed in Reference [5] is most pronounced in the regime after the 250th cycle, and consequently, seems to have no significant impact on the mechanical properties determined in CITs, and thus, cyclic hardening potential. However, crack propagation can be influenced by this "polygonization", which cannot be detected in CITs and has, hence, to be considered by evaluating the TMF-behavior.

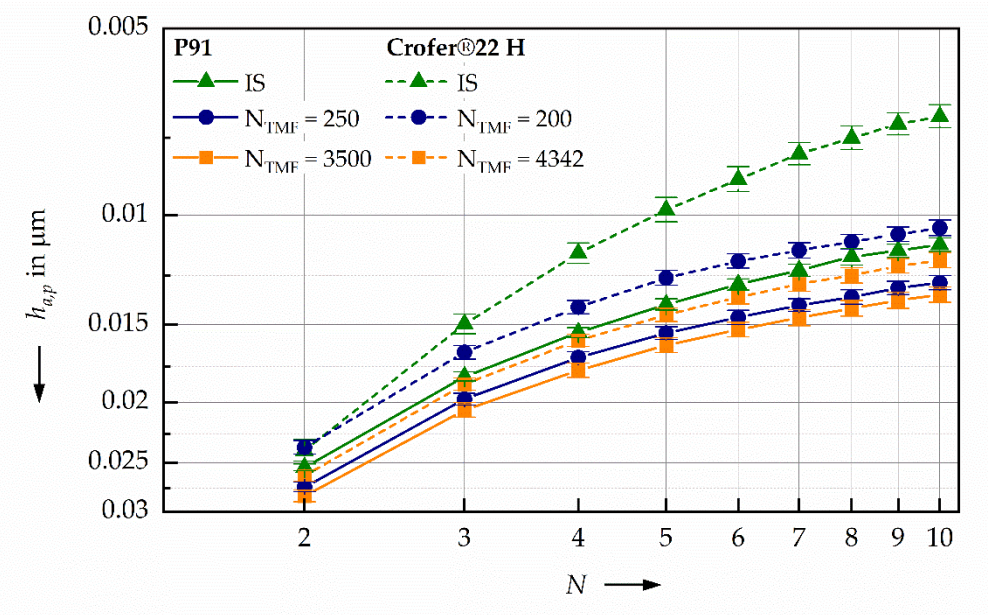

Figure 6. Comparison of the $h_{a,p}$-N curves of specimens made of P91, as well as Crofer®22 H and loaded for a different number of TMF-cycles N_{TMF}.

In CITs, CroFer®22 H exhibit a significant increase of hardness and decrease of $|e_{II}|$ in the first 20 TMF-cycles, which is accompanied by a pronounced cyclic hardening indicated by increasing stress range in Figure 3. With increasing N_{TMF}, in spite of decreasing stress range (see Figure 3), the increase in Martens hardness and decrease in cyclic hardening potential continues, leading to a maximum of hardness and minimum of $|e_{II}|$ at N_{TMF} = 1000. These extensive changes in the material properties are accompanied by a pronounced shift of $h_{a,p}$-N curves to higher values at N_{TMF} = 250 (see Figure 6), resulting in decreasing hardening potential in this condition. However, after 2000 TMF cycles, Crofer®22 H exhibits a decrease in hardness, but an increasing $|e_{II}|$. Consequently, the damage tolerance of Crofer®22 H seems to be improved within the 2nd half of TMF-lifetime, i.e., N_{TMF} > 2000. The increase of cyclic hardening potential, and hence, damage tolerance, of Crofer®22 H in this state corresponds to the prolonged damage phase in TMF-test reported in Reference [5].

To explain the results observed in CITs at Crofer®22 H, different microstructural phenomena have to be considered. Because of the massive plastic deformation at the beginning of the TMF-experiments, an increase of dislocation density, leading to smaller $|e_{II}|$ and higher hardness (see Reference [16]), is assumed. In addition to that, the results in Reference [5] demonstrate an accelerated Laves phase formation caused by TMF-loading. Note that higher dislocation density would be expected to be non-permanent in TMF-condition, but because Laves phase precipitates pin the dislocations, it is assumed to be quasi-permanent [5]. The number of the Laves phase particles significantly increases in the first 2000 cycles, and afterwards, decreases until failure, which at least roughly correlates with the hardness maximum observed in CITs, but also with the respective minimum in cyclic hardening potential (comp. Figure 5 and Reference [5]). Besides a decrease in a number of the Laves phase particles, a pronounced coarsening of the Laves phase particles can be observed at N_{TMF} > 2000, which obviously leads to an increase of $|e_{II}|$ and lower hardness.

In this context, the results of Reference [13] for precipitation hardened Cu alloyed steels show, that the hardness, as well as the cyclic hardening potential, depend on the number and size, as well as the coherency state of Cu precipitates. Consequently, the Laves phase evolution has to be considered to explain the results observed in CITs. It is assumed that the combination of the Laves phase particle evolution and cyclic plastic deformation in TMF-tests leads to the observed changes in cyclic hardening potential, as well as hardness. Future research aims to investigate the interrelation between dislocation density, Laves phase particles, and mechanical properties.

Comparing the different materials, Crofer®22 H shows more pronounced changes in hardness and $|e_{II}|$, due to TMF-loading (see Figure 5), which further can be seen in the $h_{a,p}$-N curves (see Figure 6). While P91 has a higher hardness and smaller $|e_{II}|$ in the initial state, an oop TMF-loading of approximately 1000 cycles yields higher hardness and lower cyclic hardening potential for Crofer®22 H. However, at $N_{TMF} > 2000$, Crofer®22 H shows increasing cyclic hardening potential, whereas P91 exhibits a stabilized state, underlining the higher damage tolerance of Crofer®22 H described in Reference [5]. Furthermore, the $h_{a,p}$ values obtained for Crofer®22 H are smaller compared to the ones of P91 (see Figure 6), which is less pronounced at higher N_{TMF}, demonstrating the more extensive microstructural changes of Crofer®22 H during TMF-loading.

As a summary, the results observed in CITs correspond to the cyclic deformation behavior obtained in TMF-tests. Moreover, for Crofer®22 H, microstructural changes correlate with changes in cyclic hardening potential and hardness obtained in CITs. Furthermore, the results of CITs underline the assumption, that Crofer®22 H has a significantly higher damage tolerance. Additionally, Crofer®22 H shows in relation to P91 more pronounced changes in damage tolerance during TMF-loading, i.e., an increasing cyclic hardening potential during TMF-test, leading to a longer lifetime.

4.2. Investigation of the Local Cyclic Hardening Potential and Hardness in the Vicinity of a Fatigue Crack

As shown in Reference [5] and the results of the CITs given above, the damage tolerance of Crofer®22 H is significantly higher, and TMF-induced changes are more pronounced compared to P91. Moreover, the discussion in Section 4.1 demonstrates, that the evolution of cyclic hardening potential of Crofer®22 H is strongly dependent on dislocation density and Laves phase particles, which relate to the amount of plastic deformation, being significantly higher at the crack tip. Therefore, CITs were performed at the crack edges, as well as the plastically deformed zone in front of the crack tip of a secondary fatigue crack observed at the Crofer®22 H specimen loaded for $N_{TMF} = 4342$ (see Figure 4a). These locally performed CITs enable a detailed analysis of the evolution of damage tolerance during fatigue crack propagation.

The results obtained with $F_{max} = 1000$ mN shown on the left-hand side of Figure 7, exhibit slightly higher hardness and a significantly reduced cyclic hardening potential in front of the crack tip in relation to the material's volume in the gauge length. This is assumed to be caused by more pronounced plastic deformation in front of the fatigue crack. In correspondence to that, the crack edges also show decreased cyclic hardening potential. Due to higher amounts of plastic deformation, Laves phase particle formation is assumed to be more pronounced at the crack tip and edges (see Reference [5]), which also influences hardness, as well as $|e_{II}|$ and is objective of further investigation.

To analyze the differences between the crack tip and crack edge, CITs with $F_{max} = 100$ mN were conducted, leading to a higher spatial resolution. Due to the indentation size effect (see References [16,22]), the CITs with $F_{max} = 100$ mN yield a higher hardness compared to $F_{max} = 1000$ mN (see Figure 7). By using the lower F_{max}, a higher cyclic hardening potential at the crack edges in relation to the plastically deformed volume at the crack tip can be observed. This correlates to sub-grain formation at the crack edges caused by plastic deformation during crack propagation, which is less pronounced in the plastic zone around the crack tip (see Figure 8). However, this cannot explain the decreased hardness in the vicinity of crack edges compared to the crack tip. Moreover, it has to be considered, that the areas at the crack edges were plastically deformed in an earlier state of the TMF-test. This increases the possibility of the Laves phase particle formation at dislocations, which probably also influences cyclic hardening potential and hardness. This will be the focus of the ongoing work.

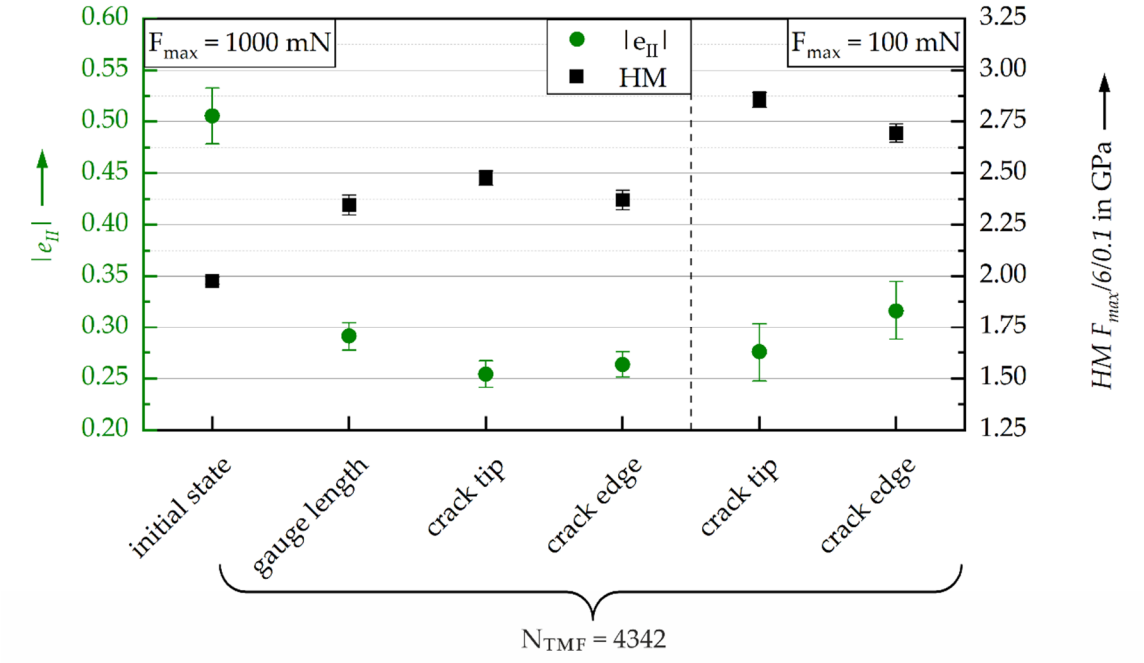

Figure 7. Cyclic hardening exponent$_{CHT}$ $|e_{II}|$ and martens hardness *HM* at the volume of the gauge length, crack edges and plastic zone in front of the crack tip at a fatigue crack observed at a Crofer®22 H specimen loaded for 4342 TMF-cycles.

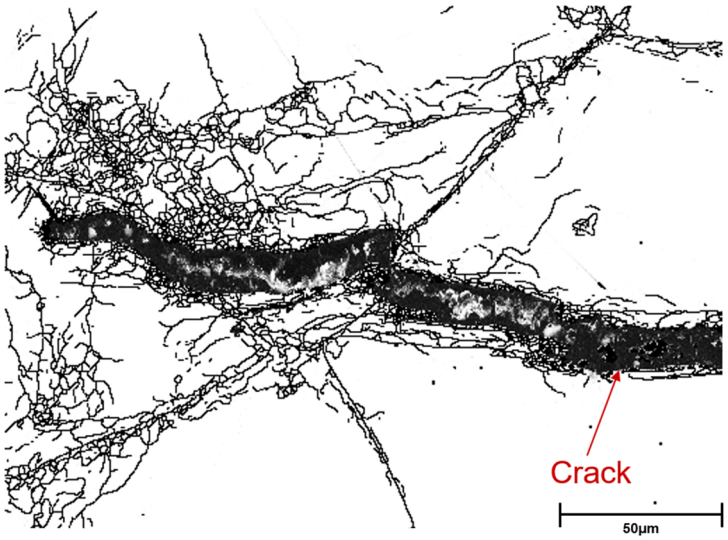

Figure 8. Sub-grain formation in ferritic Crofer®22 H, observed in the specimen, failed after 4342 TMF-cycles [5].

Conclusively, the presented investigations at the fatigue crack demonstrate, that CITs can be used to determine local differences in the material's cyclic properties, which correlates to microstructural changes observed. The evolution of the complex microstructure of Crofer®22 H in the fatigue crack vicinity, and its influence on the results obtained in CITs will be investigated intensively in future work.

5. Conclusions

In the presented work, the damage tolerance of 22 wt.% Cr, fully ferritic stainless steel Crofer® 22 H, as well as advanced ferritic-martensitic (AFM) steel P91, was analyzed using the short-time procedure PhyBaL$_{CHT}$. This was based on instrumented cyclic indentation tests (CITs), which were performed

at specimens and loaded for the different numbers of oop TMF-cycles, as well as in the vicinity of a fatigue crack in a Crofer®22 H specimen. Consequently, the presented work focuses on the evolution of damage tolerance during TMF-loading, as well as the local changes in defect tolerance in the vicinity of a fatigue crack. The following conclusions can be drawn from the results obtained:

- In the initial state, Crofer®22 H has a higher damage tolerance compared to P91, which correlates to higher TMF-lifetime;
- After approximately half of TMF-lifetime, an increase of damage tolerance can be observed for Crofer®22 H, which is not seen for P91 and correlates with changes of the Laves phase particle size and distribution;
- Polygonization, resulting from degradation of martensite lath structure in P91, does not influence the microhardness, as well as cyclic hardening potential obtained in CITs;
- For Crofer®22 H, the changes in damage tolerance correlate well with the cyclic deformation behavior observed in TMF-experiment and the accompanied microstructural changes;
- The cyclic hardening potential, and hence, damage tolerance, as well as hardness, is different between the crack tip and crack edges in Crofer®22 H;
- CITs are a powerful means to analyze the TMF-induced changes in mechanical properties, i.e., cyclic hardening potential, as well as for the investigation of locally restricted changes in the material's cyclic deformation behavior.

However, the presented work also shows that a thorough understanding between the microstructural changes (Laves phase particle evolution, dislocation density, and sub-grain boundary formation) and the resulting deformation behavior observed in CITs is a prerequisite. This will be considered in further investigations.

Author Contributions: Conceptualization, B.B., D.G., T.F., B.K. and T.B.; methodology, B.B., D.G., T.F., B.K. and T.B.; investigation, D.G. and T.F.; writing—original draft preparation, B.B., D.G. and T.F.; writing—review and editing, B.B., B.K. and T.B.; visualization, D.G.; supervision, B.B., B.K. and T.B.; project administration, B.K. and T.B.; funding acquisition, B.K. and T.B. All authors have read and agreed to the published version of the manuscript.

Funding: The financial support of the priority research activity of Rhineland Palatinate "Advanced Materials Engineering (AME)" is gratefully acknowledged.

Acknowledgments: The authors would like to acknowledge the support of B. Werner and H. Reiners in mechanical testing as well as J. Bartsch for metallographic preparation and E. Wessel and D. Grüner for microstructural characterization work.

Conflicts of Interest: The authors declare no conflict of interest.

References

1. Holdsworth, S. Creep-Fatigue Crack Growth in Power Plant Steels. *Trans. Indian Inst. Met.* **2015**, *69*, 353–358. [CrossRef]
2. Kuhn, B.; Talik, M.; Zurek, J.; Beck, T.; Quadakkers, W.J.; Singheiser, L.S. Development of High Chromium Ferritic Steels Strengthened by Intermetallic Phases. In Proceedings of the Seventh International Conference of Advances in Materials Technology for Fossil Power Plants, Waikoloa, HI, USA, 22–25 October 2013.
3. Pandey, C.; Mahapatra, M.M.; Kumar, P.; Saini, N. Some studies on P91 steel and their weldments. *J. Alloys Compd.* **2018**, *743*, 332–364. [CrossRef]
4. Kuhn, B.; Talik, M.; Niewolak, L.; Zurek, J.; Hattendorf, H.; Ennis, P.; Quadakkers, W.J.; Beck, T.; Singheiser, L. Development of high chromium ferritic steels strengthened by intermetallic phases. *Mater. Sci. Eng. A* **2014**, *594*, 372–380. [CrossRef]
5. Kuhn, B.; Barrilao, J.L.; Fischer, T. Impact of Thermomechanical Fatigue on Microstructure Evolution of a Ferritic-Martensitic 9 Cr and a Ferritic, Stainless 22 Cr Steel. *Appl. Sci.* **2020**, *10*, 6338. [CrossRef]
6. Kuhn, B.; Talik, M.; Fischer, T.; Fan, X.; Yamamoto, Y.; Barrilao, J.L. Science and Technology of High Performance Ferritic (HiperFer) Stainless Steels. *Metals* **2020**, *10*, 463. [CrossRef]
7. Mughrabi, H. Cyclic Slip Irreversibilities and the Evolution of Fatigue Damage. *Met. Mater. Trans. A* **2009**, *40*, 431–453. [CrossRef]

8. Link, R.; Yang, L.; Fatemi, A. Cumulative Fatigue Damage Mechanisms and Quantifying Parameters: A Literature Review. *J. Test. Eval.* **1998**, *26*, 89–100. [CrossRef]
9. Lemaitre, J.; Dufailly, J. Damage measurements. *Eng. Fract. Mech.* **1987**, *28*, 643–661. [CrossRef]
10. Šulko, M.; Vladimír, C.; Kepka, M. Possibility of fatigue damage detection by non-destructive measurement of the surface hardness. *Procedia Struct. Integr.* **2017**, *7*, 262–267. [CrossRef]
11. Liu, M.; Lin, J.-Y.; Lu, C.; Tieu, K.; Zhou, K.; Koseki, T. Progress in Indentation Study of Materials via Both Experimental and Numerical Methods. *Crystals* **2017**, *7*, 258. [CrossRef]
12. Hay, J.L.; Pharr, G.M. Instrumented Indentation Testing. In *Mechanical Testing and Evaluation*, 11th ed.; Kuhn, H., Ed.; ASM International: Geauga County, OH, USA, 2000; pp. 231–242. ISBN 0871703890.
13. Görzen, D.; Schwich, H.; Blinn, B.; Bleck, W.; Beck, T. Influence of different precipitation states of Cu on the quasi-static and cyclic deformation behavior of Cu alloyed steels with different carbon contents. *Int. J. Fatigue* **2020**, *136*, 105587. [CrossRef]
14. Saraswati, T.; Sritharan, T.; Mhaisalkar, S.G.; Breach, C.; Wulff, F. Cyclic loading as an extended nanoindentation technique. *Mater. Sci. Eng. A* **2006**, *423*, 14–18. [CrossRef]
15. Kramer, H.S.; Starke, P.; Klein, M.; Eifler, D. Cyclic hardness test PHYBALCHT – Short-time procedure to evaluate fatigue properties of metallic materials. *Int. J. Fatigue* **2014**, *63*, 78–84. [CrossRef]
16. Blinn, B.; Görzen, D.; Klein, M.; Eifler, D.; Beck, T. PhyBaL_{CHT}—Influence of indentation force on the results of cyclic hardness tests and investigations of comparability to uniaxial fatigue loading. *Int. J. Fatigue* **2019**, *119*, 78–88. [CrossRef]
17. Blinn, B.; Ley, M.; Buschhorn, N.; Teutsch, R.; Beck, T.; Blinn, B. Investigation of the anisotropic fatigue behavior of additively manufactured structures made of AISI 316L with short-time procedures PhyBaL_{LIT} and PhyBaL_{CHT}. *Int. J. Fatigue* **2019**, *124*, 389–399. [CrossRef]
18. Blinn, B.; Krebs, F.; Ley, M.; Teutsch, R.; Beck, T. Determination of the influence of a stress-relief heat treatment and additively manufactured surface on the fatigue behavior of selectively laser melted AISI 316L by using efficient short-time procedures. *Int. J. Fatigue* **2020**, *131*, 105301. [CrossRef]
19. Durst, K.; Backes, B.; Göken, M. Indentation size effect in metallic materials: Correcting for the size of the plastic zone. *Scr. Mater.* **2005**, *52*, 1093–1097. [CrossRef]
20. Sadrabadi, P.; Durst, K.; Göken, M. Study on the indentation size effect in CaF2: Dislocation structure and hardness. *Acta Mater.* **2009**, *57*, 1281–1289. [CrossRef]
21. Klein, M.W.; Blinn, B.; Smaga, M.; Beck, T. High cycle fatigue behavior of high-Mn TWIP steel with different surface morphologies. *Int. J. Fatigue* **2020**, *134*, 105499. [CrossRef]
22. Nix, W.D.; Gao, H. Indentation size effects in crystalline materials: A law for strain gradient plasticity. *J. Mech. Phys. Solids* **1998**, *46*, 411–425. [CrossRef]
23. Masuyama, F. Advances in Physical Metallurgy and Processing of Steels. History of Power Plants and Progress in Heat Resistant Steels. *ISIJ Int.* **2001**, *41*, 612–625. [CrossRef]
24. Pandey, C.; Giri, A.; Mahapatra, M. Evolution of phases in P91 steel in various heat treatment conditions and their effect on microstructure stability and mechanical properties. *Mater. Sci. Eng. A* **2016**, *664*, 58–74. [CrossRef]
25. Quadakkers, W.J.; Wijnandsrade, N.L.; Niewolak, L.; Ennis, P.J. Kriechfester Ferritischer Stahl (Creep-Resistant Ferritic Steel). Patent DE102006007598A1, 30 August 2007.
26. Schiller, G.; Franco, T.; Henne, R.; Lang, M.; Szabo, P.; Finkenwirth, O.; Kuhn, B.; Wetzel, F.-J. Development of Thin-Film SOFC for Stationary and Mobile Application by Using Plasma Deposition Technology. *ECS Proc. Vol.* **2003**, 1051–1058. [CrossRef]
27. Froitzheim, J.; Meier, G.; Niewolak, L.; Ennis, P.; Hattendorf, H.; Singheiser, L.; Quadakkers, W.J. Development of high strength ferritic steel for interconnect application in SOFCs. *J. Power Sources* **2008**, *178*, 163–173. [CrossRef]
28. Hsiao, Z.-W.; Kuhn, B.; Chen, D.; Singheiser, L.; Kuo, J.-C.; Lin, D.-Y. Characterization of Laves phase in Crofer 22 H stainless steel. *Micron* **2015**, *74*, 59–64. [CrossRef]
29. Hsiao, Z.W.; Kuhn, B.; Yang, S.M.; Yang, L.C.; Huang, S.Y.; Singheiser, L.; Kuo, J.C.; Lin, D.Y. The Influence of Deformation on the Precipitation Behavior of a Ferritic Stainless Steel. In Proceedings of the 10th Liége Conference on Materials for Advanced Power Engineering, Liége, Belgium, 14–17 September 2014; Lecomte-Beckers, J., Dedry, O., Oakey, J., Kuhn, B., Eds.; pp. 349–358.

30. Pöpperlová, J.; Fan, X.; Kuhn, B.; Bleck, W.; Krupp, U. Impact of Tungsten on Thermomechanically Induced Precipitation of Laves Phase in High Performance Ferritic (HiperFer) Stainless Steels. *Appl. Sci.* **2020**, *10*, 4472. [CrossRef]
31. Madyira, D.M.; Liebenberg, J.; Kaymacki, A. Comparative Characterization of P91 and 10CrMo9-10 Creep Resistant Steel Welds. *Procedia Manuf.* **2017**, *8*, 345–352. [CrossRef]
32. Crofer®22 H. *Material Data Sheet No. 4050*; ThyssenKrupp VDM GmbH: Werdohl, Germany, June 2010.
33. Hähner, P.; Affeldt, E.; Beck, T.; Klingelhöffer, H.; Loveday, M.; Rinaldi, C. *Validated Code-of-Practice for Thermo-Mechanical Fatigue Testing*; Joint Research Centre: Luxembourg, 2006.
34. Besel, M.; Breitbarth, E. Advanced analysis of crack tip plastic zone under cyclic loading. *Int. J. Fatigue* **2016**, *93*, 92–108. [CrossRef]